Title

Synchronized Minima in ECoG Power at Frequencies Between Beta-Gamma Oscillations Disclose Cortical Singularities in Cognition

Permalink

https://escholarship.org/uc/item/9ht4t9d6

Journal

Journal of Neuroscience and Neuroengineering, 1(1)

Authors

Kozma, Robert
Davis, Jeffery Jonathan (Joshua)
Freeman, Walter J, III

Publication Date

2012-07-27

Copyright Information

This work is made available under the terms of a Creative Commons Attribution License, availalbe at https://creativecommons.org/licenses/by/3.0/

Peer reviewed

Synchronized Minima in ECoG Power at Frequencies Between Beta-Gamma Oscillations Disclose Cortical Singularities in Cognition

Robert Kozma[1,*], Jeffery Jonathan (Joshua) Davis[1,2], and Walter J. Freeman[3]

[1]Center for Large-Scale Integrated Optimization Networks Department Mathematical Sciences,
University of Memphis, Memphis, TN 38152, USA
[2]Embassy of Peace, Whitianga, 3542, New Zealand
[3]Molecular and Cell Biology, Division of Neurobiology University of California at Berkeley, CA 94720, USA

Electrocorticogram (ECoG) data of trained rabbits are analyzed to identify neural correlates of cognition. Previous work indicated long periods of large-scale synchronization of cortical activity, punctuated intermittently by brief desynchronization events. The actual timing of the synchronization events generally depends on the analyzed frequency band, from alpha to high gamma. Here we present the surprising experimental indications that the desynchronization events may synchronize briefly over a wide range of frequencies during a singular event of cognition. The observed synchronization of desynchronization (SOD) effect has significant invariance over broad frequencies. This observation is in line with the expected scale-free behavior of critical brain dynamics. To quantify the observed SOD phenomenon, we analyze information-theoretic measures based on the concept of pragmatic information, to complement the Shannon entropy index. We demonstrate the benefit of the new indices in the analysis and detection of phase transitions and possible desynchronization windows in time domain. The results are interpreted in terms of a dynamical system approach to brains operating in a domain of criticality.

KEYWORDS: Electrocorticogram (ECoG), Hilbert Transform, Synchronization, Criticality, Singularity, Cognition.

INTRODUCTION

Neurophysiological processes manifesting higher cognition and consciousness are intensively studied worldwide and there are great many spectacular successes in the field; see, e.g., Refs. [1–5]. A word of caution is in place in the interpretation of the experimental findings. Brains are the most complex substances in the known Universe and only the most advanced brain imaging methods with the highest spatial and temporal resolution can give hope for deciphering the language of the brain.

A potential trap in modeling and interpreting the operation of brains is characterized by philosopher H. Dreyfus as *representational cognitivism* [6–7]. According to Dreyfus, representational cognitivism tries to identify localized handles as components of a symbol system describing brains and their intelligent operation. These symbols, however, are not grounded in the neurophysiology of the brain according to Dreyfus, rather they represent just a pile of meaningless facts irrelevant to the cognitive functions of the brain. Representational cognitivism is unable to solve the framing problem and cannot provide meaningful support to the individual, either biological (animal/human) or artificial (animat). *Embodied cognition* has been proposed as a promising approach to resolve this controversy [8–10].

Nonlinear neurodynamics addresses this challenge by viewing the brain as a dynamical system and it has been used successfully to interpret embodied cognition and learning in neural systems [11–17]. Dynamic models can provide the causal basis of the adaptive ability of brains and give an account of how the brain of an active animal can directly pick up and update what counts as significant in its world [6, 18]. In the neurodynamic approach to cognition, learning establishes an attractor landscape over each cortical area, in which the basins of attraction are shaped by experience. Each attractor in the landscape corresponds to a class of stimulus that the animal has learned to discriminate, and each attractor is accessed by the arrival of a learned stimulus of that class. A systematic formulation of dynamical brain theory is expressed in Freeman K (Katchalsky) sets [11, 19–20].

Synchronization effects play a key role in cortical functions and numerous brain studies are currently in

*Author to whom correspondence should be addressed.
Email: rkozma@memphis.edu

progress to evaluate the levels of synchrony across large cortical populations. Intermittent synchronization-desynchronization has been modeled using K-sets, and an experimental paradigm has been outlined to construct a distributed decision support systems based on such principles [21–22]. In consequent work [23–24] it has been hypothesized that phase transitions are the hallmarks of higher cognition and awareness [25]. If the brain indeed exhibits critical phase transitions in line with that hypothesis, then scale-free behavior is expected to take place during cognitive states near criticality. Such scale-free behavior should include time dimension, spanning across a range of frequencies. Until now there has not been sufficient evidence to support this hypothesis.

In the present work we introduce experimental results on synchronization effects across a range of temporal frequency bands. The work reported here is based on experimental ECoG studies using intracranial electrode arrays implanted in rabbits [21]. Previous studies were limited to specific frequency bands, such as gamma or theta band. Here we give comprehensive analysis for broader frequencies. We start with describing ECoG experiments with rabbits, followed by introducing the Hilbert transform-based signal processing method. Our results point to a clear synchronization effect as a specific time instant across frequencies covering delta-, theta-, alpha-, beta-, and gamma bands. This time instant marks intensive cognitive activity, i.e., classification of previously learnt conditioned stimuli by the rabbit. We quantify the obtained results using information-theoretic measures and discuss their relevance to the characterization of cognitive functions. We conclude with the description of future plans and perspectives.

DESCRIPTION OF RABBIT ECoG EXPERIMENTS

Electrical activity of rabbit cortices has been measured using an array of 8×8 clinically implanted electrodes [9]. The space between the electrodes is 0.8 mm covering an area of 5.6 mm * 5.6 mm in either of the olfactory, visual, auditory or somatomotory cortices [21], see Figure 1. Here, experiments on the visual cortex are analyzed. Experiments have been conducted for a duration of 6 s, which have been divided into 3 s pre-stimulus and 3 s post-stimulus periods. The sampling frequency was 500 Hz, which gave a total of 3000 sample points for each of the 64 channels. The rabbits were trained to discriminate visual conditioned stimuli eliciting conditioned responses, which have been analyzed during the 3 s post-stimulus time segments. During data recording, the signals were low-pass filtered at 100 Hz.

Local areas of sensory cortices generate broad-spectrum, aperiodic waves of dendritic activity that have the same waveform, which is observed as the similarity of the amplitude modulation (AM) patterns of EEGs channels recorded by the electrode array. The AM patterns are
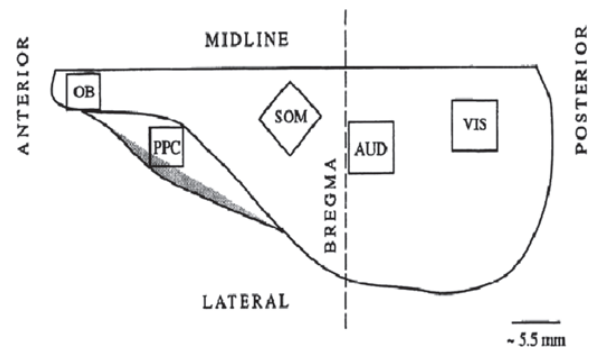

Fig. 1. Illustration of the arrangement of the 8×8 electrode arrays at various implant sites on the cortex. In the present study we analyze data observed by visual experiments; Adopted with permission from [21], J. M. Barrie et al., Modulation by discriminative training of spatial patterns of gamma EEG amplitude and phase in neocortex of rabbits. *J. Neurophysiol.* 76, 520 (**1996**). © 1996, Amer. Physiol. Soc.

determined by the synaptic connectivity within each cortex, which change with the training of animals to identify significant stimuli. Evidence for the dynamic systems theory in cortices comes from the results of classification of the spatial AM patterns. The EEG segments coming from a sensory area give clusters of points, each of which corresponds to a response to a sample of the class of stimulus that the animal has learned to identify. Discrimination is learned by the animal under classical conditioning paradigm, in which one stimulus is reinforced (CS+) and the other is not (CS−).

In order to establish a baseline level of classification, EEGs recorded from a sensory area are segmented by fixed-length windows (64 ms) stepped at fixed-length time intervals (32 ms) into a matrix. As a result, we have a sequence of AM patterns measured at regular intervals, 32 ms in the present case. These AM patterns provide all the knowledge we have on the operation of the cortex at the given level of spatial and temporal granularity.

Sequential AM patterns evidence the occasional onset of phase cones, which evolved starting at some time instant from some spatial point. The onset time and starting apex point of the cones occur at an apparently arbitrary point in space-time. Thereafter a phase gradient propagates from the apex rapidly, at a speed comparable to the speed of neural signal propagation along lateral axons in the cortical neuropil [22–23]. Phase cones serve as markers, by which to locate the starting and ending times of emergent AM patterns having randomly varying latencies over sequential trials in which either of two discriminated stimuli were presented, one reinforced and the other not. Before classification, the AM patterns are pre-processed based on the observed onset time of phase cones. In addition, a model-based filtering has been applied using K-set (KIII) [19, 23]. The statistical significance of the AM pattern classification has been evaluated using Student's t-test.

The null hypothesis (H0) states that the observed AM pattern is undistinguishable with respect to the
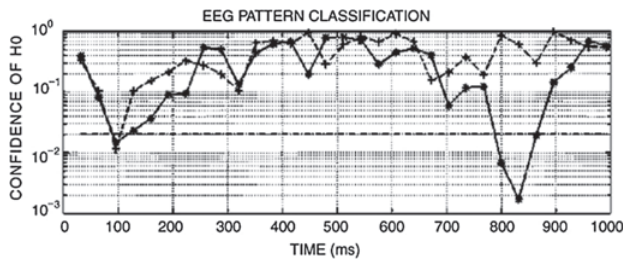
Fig. 2. Temporal variation of the confidence level of the zero hypothesis (H0), which states that the observed AM patterns are not distinguishable with respect to the conditioned stimuli. H0 can be rejected for a short period after the stimulus (at $t = 0$), and also in the time window around 750–850 ms. *Dash*: without preprocessing; *Solid line*: with advanced preprocessing using phase cone detection. Reprinted with permission from [23], R. Kozma and W. J. Freeman, Classification of EEG patterns using nonlinear neurodynamics and chaos. *Neurocomputing* 44–46, 1107 (**2002**). © 2002, Elsevier.

classification measures concerning CS+ and CS−. The alternative hypothesis (H1) states that the observed AM pattern is closer to its correct cluster, thus it is distinguishable using the given classification tool. This method yields a sequence of probability values showing the times when the CS− and CS+ spatial AM patterns can and cannot be separated. Separation does not occur in the 3 s control period before the stimulus.

The analysis reveals two types (Type I and Type II) of discriminable AM patterns in the (visual) sensory cortex during the post-stimulus period [23]. Type I occurs with short latency after the stimulus (within 200 ms). Type I AM pattern represents the direct impact of a discriminated stimulus on the activity of the receiving cortex. Type II classifiable AM pattern is delayed and it occurs with variable latency within 300–1000 ms of the stimulus onset. It is endogenous and the result of complex transformations through the divergent-convergent neural pathways. Its location in time is revealed by a phase cone at the center frequency of the gamma oscillation. Type II AM pattern has been interpreted as the indication of chaotic self-organization of cortical dynamics as the result of sensory input-induced destabilization.

In the past decade, Hilbert transform-based analytic signal evaluation method became widely used in EEG studies, due to the fine temporal resolution provided by this approach. In the follow discussions, we employ such analytic approach to the rabbit ECoG data and introduce the results which shed light on the details of the spatio-temporal dynamics, especially following the stimulus.

HILBERT ANALYSIS OVER THE THETA BAND

Analytic Amplitude and Phase Relationships of ECoG Signals

We calculate analytic signals $V(t)$ after Hilbert-transforming the 64-channel ECoG array data. The applied

Hilbert transform methodology follows the approach described in [26–27]. The EEG of each channel $v_j(t)$ ($j = 1, \ldots, 64$) is transformed to a time series of complex numbers, $V_j(t)$, with a real part, $v_j(t)$, and an imaginary part, $u_j(t)$,

$$V_j(t) = v_j(t) + iu_j(t), \quad j = 1, 64 \quad (1)$$

Here the real part is the EEG signal, while the imaginary part is the Hilbert transform of $v_j(t)$. We use MATLAB 'hilbert' function to produce $u_j(t)$. Sequences of steps give a trajectory of the complex vector $V(t)$ composed of 64 complex values evolving in time. The vector length at each digitizing step, t, is the analytic amplitude:

$$A_j(t) = [v_j^2(t) + u_j^2(t)]^{.5} \quad (2)$$

while the analytic phase is defined and the arctangent of the angle of the vector:

$$P_j(t) = \text{atan}[u_j(t)/v_j(t)] \quad (3)$$

In this section, we show detailed results obtained in the theta band. This helps to illustrate major features of Hilbert analysis. In the next section we introduce results over a broad range of frequencies.

Band-pass filter is applied in the theta band with parameters: $F_{stopL} = 3$ Hz, $F_{passL} = 4$ Hz, $F_{passH} = 6$ Hz, and $F_{stopH} = 7$ Hz. Figure 3 shows filtered ECoG signals for all 64 channels (top), the analytic phase of the signals after Hilbert transform (middle), and the absolute analytic frequency derived from the instantaneous phase differences (bottom).

Figure 3 shows that the channels move together and highly synchronized most of the time. During these prolonged synchronized periods the spatial mean analytic frequency is constant at the center frequency of the pass band and it is concentrated near the applied pass band of 4 Hz–6 Hz. From time to time, there are moments with significant dispersion of the signal amplitudes and phases. The loss of synchrony is clearly visible through the spikes in the analytic frequency, e.g., at time instants 1.2s, 2.8 s, 3.1 s, 3.5 s, and so on. At these time instances the synchronization between channels breaks down, which dispersion will be used as an indicator of the indeterminacy of analytic phase during the times of marked decrease in analytic amplitude.

Figure 4 combines analytic amplitudes (blue) with instantaneous frequencies (red). Visual inspection indicates that events marked by spikes in the instantaneous phase mostly coincide with drops in the analytic amplitudes. This is in agreement with earlier finding using ECoG and EEG data [26–27]. There are exceptions from this rule. For example, just before 3 s, the amplitude drops close to zero, but the instantaneous phase does not exhibit a spike. Similar behaviors are observed over all frequency bands,
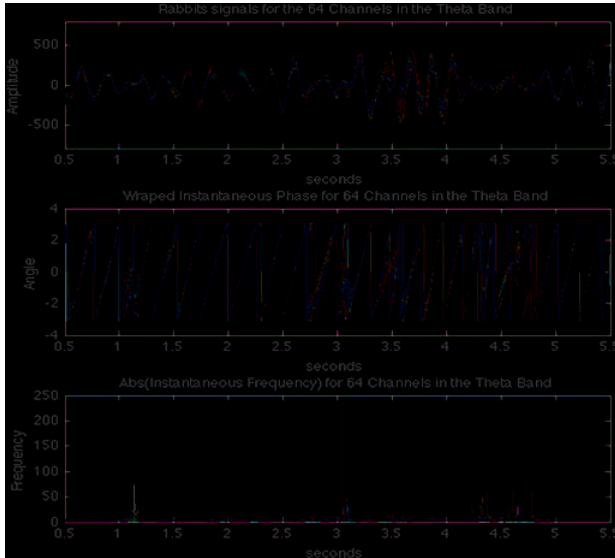
Fig. 3. Illustration of the analyzed rabbit ECoG data filtered over theta band with pass band 4 Hz to 6 Hz. Top diagram: signals of all 64 channels; middle: analytic phase of the signals after Hilbert transform; bottom: absolute analytic frequency derived from the instantaneous phase differences.

which will be presented in the next section together with its quantitative characterization.

The events occurring before 3 s and after 4 s seem to have a different influence on the amplitude than the events occurring between the 3.5 s–3.8 s window. This specific window corresponds to the post-stimulus period when the rabbit's cognitive activity is the highest, following conditioned learning. In this time window, $A(t)$ exhibits complex behavior; some $A_j(t)$ channels go up, while others decrease, instead of all channels uniformly moving in the same direction. We observe that this is the period for which the signal amplitude range of the signal is the highest. Next, we develop statistical indices to quantify these behaviors.
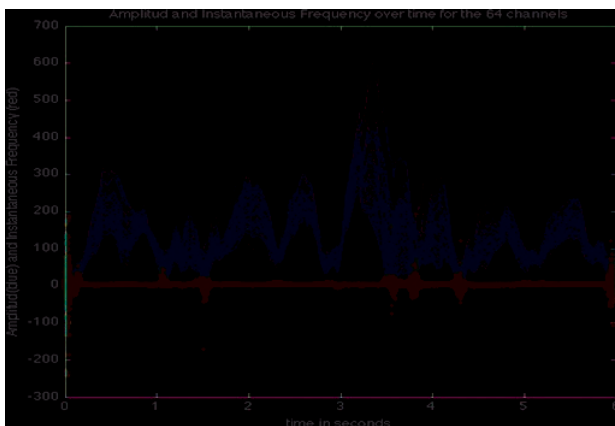
Fig. 4. Illustration of the correlation between the drops in analytic amplitude (blue) and spike in instantaneous frequency (red) for all 64 channels; theta-band analysis with pass band of 4 Hz–6 Hz.

Information-Theoretic Indices

In this section we develop a qualitative characterization of the empirically observed onization effect described previously. We describe the pragmatic information index following [29–31]; then we introduce several modified versions of the original indices [28]. We denote the 64 scalar values of the squared analytic amplitude as $A_j^2(t)$, which form a vector at each time step $A^2(t)$. Vector $A^2(t)$ serves as an order parameter. The rate of pattern evolution is proportional to the Euclidean distance, $D_e(t)$, between successive time points:

$$D_e(t) = \text{dist}(A^2(t), \quad A^2(t-1)) = |A^2(t) - A^2(t-1)| \tag{4}$$

The ratio of mean rate of free energy dissipation across the array $\langle A^2(t) \rangle$, to the rate of change in the order parameter, $D_e(t)$, defines a quantity, called pragmatic information [30]:

$$H_e(t) = <A^2(t)>/D_e(t) \tag{5}$$

Here $\langle\rangle$ denotes the spatial ensemble average. In additional to the individual channels, we define the average over $k = 8$ groups of channels, defined as follows: group $1 = \{$for channels $j = 1{:}8\}$, group $2 = \{j = 9{:}16\}, \ldots$, group $8 = \{j = 57{:}64\}$. These group averages will be useful to display the variation of the indices over the array, without giving details of individual channels. Following are the indexes relevant to our analysis:

- *Range (max-min) of Amplitude* (RA_j) for each channel. The Range of Amplitude can be the squared analytic amplitude as originally introduced by Freeman [26]; we will also evaluate indices using the signal amplitude, and the analytic amplitude.
- *Euclidean Distance*: can be calculated either for the whole lattice (D_e) or for each of the k groups (D_{ek}). This quantity has been calculated originally using analytic amplitudes as in Eq. (4); it can be calculated also using the analytic phase values.
- *Shannon Entropy Index* (SH_j) for each channel. This quantity is computed with MATLAB entropy index function.

From Refs. [30–31] we introduce the general form of Pragmatic Information Index ($H_e * (t)$) as follows:

$$H_e * (t) = \langle RAj(t) \rangle / D_e(t) \tag{6}$$

We experiment with alternative definitions of the Pragmatic Information Index, by using 3 variants of the amplitude measure. RA can be RSA, RAA, or MA2, as defined below:

- RSA(t): The Range of the Signal Amplitude;
- RAA(t): The Range of the Analytical Amplitude;
- SAA(t): The Squared Analytical Amplitude.

Each of these quantities can be defined as spatial ensemble average for the whole array, or for a specific group k. They implement either temporal average over a specific interval T for $\text{SAA}_T(t)$, $\text{RSA}_T(t)$ and $\text{RAA}_T(t)$, or can use instantaneous values in the case of $\text{SAA}(t)$. Accordingly, the following Pragmatic Information Indices are introduced:

$$\text{HRSA}_{k,T}(t) = < \text{RSA}_{k,T}(t) > /D_e(t), \qquad (7)$$

$$\text{HRAA}_{k,T}(t) = < \text{RAA}_{k,T}(t) > /D_e(t), \qquad (8)$$

$$\text{HSAA}_{k,T}(t) = < \text{SAA}_{k,T}(t) > /D_e(t) \qquad (9)$$

Note that $\text{HSAA}_{k,T}(t)$ coincides with the original definition of $H_e(t)$ in Eq. (5), if we take the instantaneous value without temporal averaging, and if the spatial average includes the whole array, not only a specific subgroup k. $\text{HRSA}_{k,T}(t)$ and $\text{HRAA}_{k,T}(t)$ introduce alternative quantities, which involve granulation in space through groups k and also granulation in time through average range evaluations over period T.

Figure 5 shows the Pragmatic Information Index $\text{HSAA}_{k,T}(t)$ calculated using Eq. (9) over 50 consecutive time segments of duration 0.1 s in the interval 0.5 s to 5.5 s. The applied frequency band is theta (4 Hz to 6 Hz). The top figure shows the spatial group indices for all k values; the bottom figure illustrates the ensemble average index over the whole array. Clearly, the index has periods of significant increase and consequent drop over the studied time window.

Figure 6 shows the Pragmatic Information Index $\text{HRSA}_{k,T}(t)$ calculated using Eq. (7) for the mean of the signal amplitudes over theta band; notations are similar to Figure 5. Finally, Figure 7 shows the $\text{HRAA}_{k,T}(t)$ index based on the mean range of analytic amplitudes (AA)
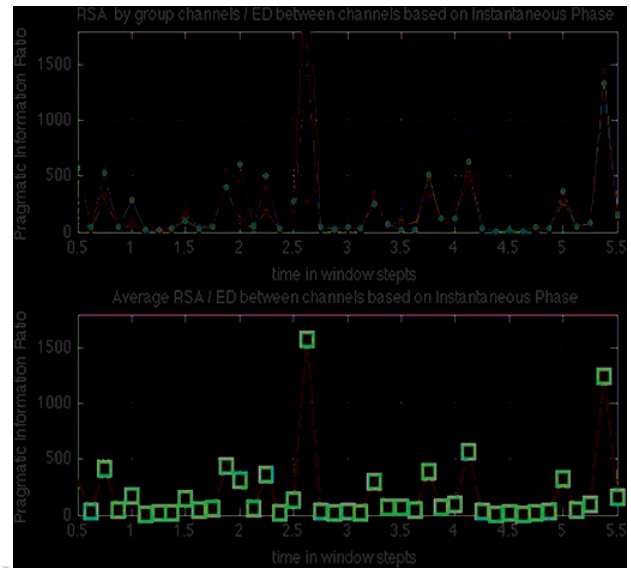
Fig. 6. Pragmatic Information Index $\text{HRSA}_{k,T}(t)$ calculated using the range of the original signal amplitudes over the theta band (4 Hz–6 Hz); top: group indices for the 7 groups; bottom:ensemble average index over the whole array.

over theta band. All the indices show spikes at given time instances. These spikes have some common features across index types, but they are not identical. Clearly, they reflect various aspects of the underlying brain dynamic process. In order to understand the underlying processes better, we depict various components of these indices for each group of channels in Figure 8; namely the Shannon Index, Amplitude measure $\text{HRAA}_{k,T}(t)$, and Euclidean distance. All these measures show changes during the analyzed period. The Shannon entropy and Euclidean distance varies significantly between the channels practically for the
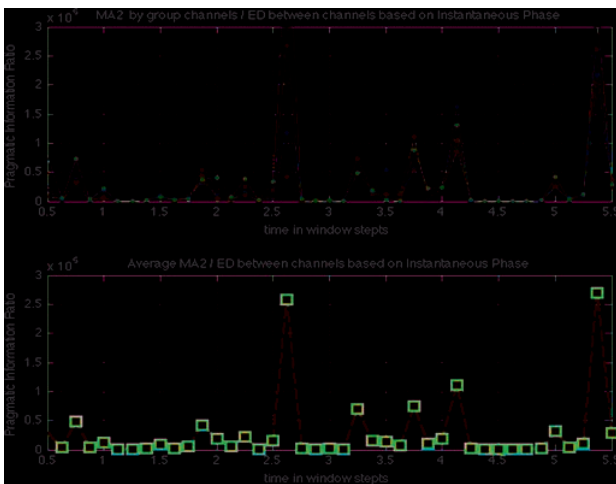

Fig. 5. Pragmatic Information Index $\text{HSAA}_{k,T}(t)$ calculated using the squared mean of analytic amplitudes over the theta band (4 Hz–6 Hz); top: group indices for the k groups, $T = 0.1$ s; bottom:ensemble average index over the whole array.
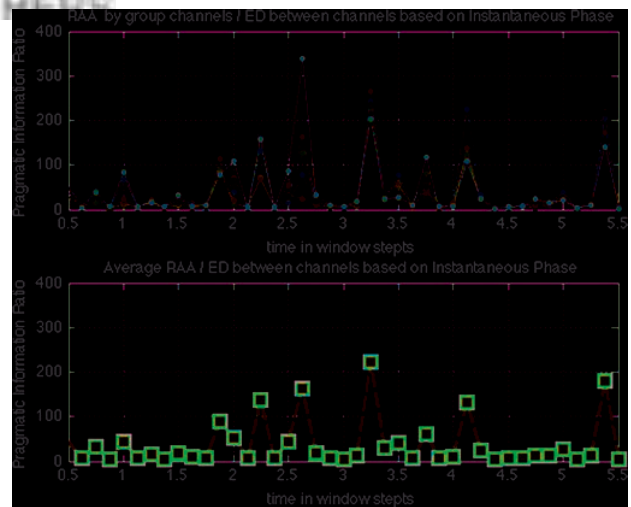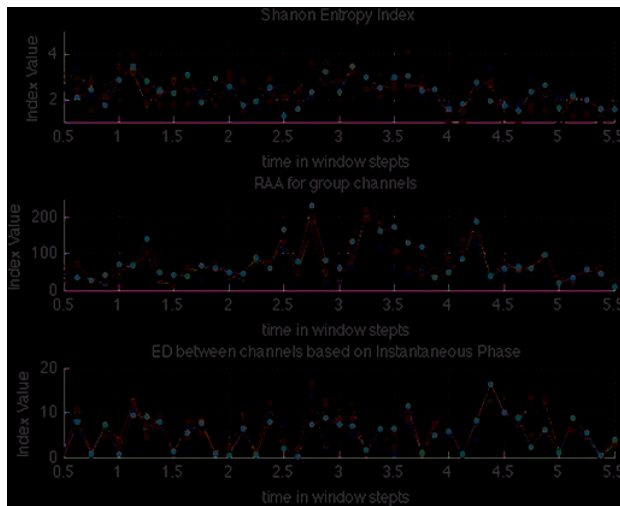

Fig. 7. Pragmatic Information Index $\text{HRAA}_{k,T}(t)$ calculated using the mean of the range of analytic amplitudes over the theta band (4 Hz–6 Hz); top: group indices for the 7 groups; bottom: ensemble average index over the whole array.

Fig. 8. Indices for the individual groups of channels calculated over 50 times steps, each of duration 0.1 s; theta band (4 Hz to 6 Hz). Shannon Entropy Index (top), Amplitude measure using range of Analytic Amplitude $HRAA_k(t)$ (middle), and Euclidean Distance.

whole experiment. The amplitude measure $HRAA_{k,T}(t)$, however, is rather uniform across all groups for most of the experiment, with the exception of the time period 3 s to 4 s. This is potentially valuable observation, as rabbits perform the classification task exactly during this time period. Similar observation is true for the other amplitude measures. The observed spatial diversity of amplitude measures and their sensitivity to cognitive activity indicates that synchronization across the cortex is closely related to cognition and decision making. Synchronization across space at various frequency bands is analyzed in the rest of this paper.

SYNCHRONIZATION STUDIES ACROSS FREQUENCY BANDS

Here we describe our findings on synchronization in space at various frequency bands, which extend previous results over the theta frequencies. In all evaluations, we keep the frequency bandwidth constant at 2 Hz, while shifting the center frequency of the filter stepwise at 2 Hz increments. The considered frequency windows are summarized in Table I.

Table I. Frequency windows analyzed.

Frequency band	Windows (Hz) f_{Low}–f_{High}
Delta	2–4
Theta	4–6, 6–8
Alpha	8–10, 10–12
Beta	12–14, 14–16, 16–18, 18–20, 20–22, 22–24, 24–26
Low gamma	26–28, 28–30, 30–32, 32–34, 34–36, 36–38, 38–40

The following quantities have been evaluated both for the band-passed ECoG and their analytic counterparts:

• *Average Signal Amplitude (SA or AA):* This can be either the amplitude of the ECoG signal (SA) or the analytic amplitude (AA) of the analytic signal calculated as ensemble average for the array.

• *Standard Deviation in Space (STDx):* The standard deviation calculated across the 64 channels for SA or AA, respectively.

• *Instantaneous Frequency (IFx):* Evaluated using the temporal derivative of the analytic phase (AP) and depicted as spatial average IF across all channels.

The results for delta, theta, and alpha bands are shown in Figures 9 and 10, describing SA and AA characteristics, respectively. Figures 11 and 12 show results for beta and low-gamma bands, where SA and AA characteristics are described, respectively. The instantaneous frequency IFx has been calculated as the spatial average over all channels. Recall that in all figures the first half of the time series corresponds to the resting period prior the stimulus, which is administered in the form of a light flash at moment $t = 3$ s. The second part of the experiments after 3 s represents the post-stimulus response. The first and last 0.5 s are omitted as those periods are used for the proper widowing. We have the following major observations based on Figures 9–12:

(1) *SA and AA:* There are significant oscillations during the whole time period, even during the resting period, but the oscillations show drastic increase between 3–4 s, i.e., immediately after the stimulus. In the case of SA, the increased amplitude is more visible at higher frequencies. For the AA, on the other hand, the increase is very prominent over all frequencies.

(2) *In the case of AA*: We can observe a fine structure of the amplitude measure. Namely, there is an increase of AA between 3–3.5 followed by a drop between 3.5–4 seconds. In this last period we can observe a small increase between 3.5–3.75 seconds, followed by a drop between 3.75–4 seconds.

(3) *STDx for SA and AA:* Here the most important feature is the overall significant increase of STDx between 3–4 seconds. This effect is clear in both SA and AA analysis.

(4) *IFx:* We consider the absolute value of IF in linear and log coordinates. We observe a drop between 3–3.5 s followed by an increase between 3.5–4 s.

(5) *AA and IFx relationship:* As a general trend, whenever there is a drop in IFx there is an increase in AA and vice versa; this is in line with previous research [26, 29]. Now we can confirm this as a general behavior over broad frequencies.
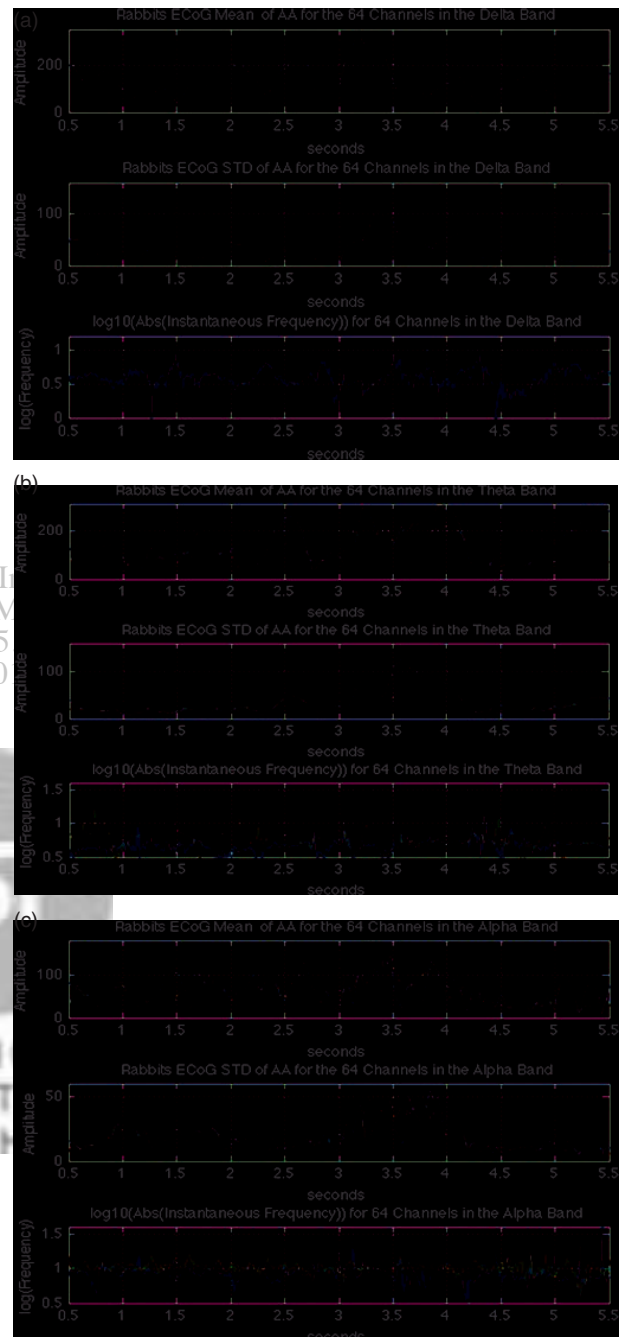
DISCUSSIONS

Based on the introduced experimental findings, we can make some important remarks. Clearly, the period between

FEATURED ARTICLE
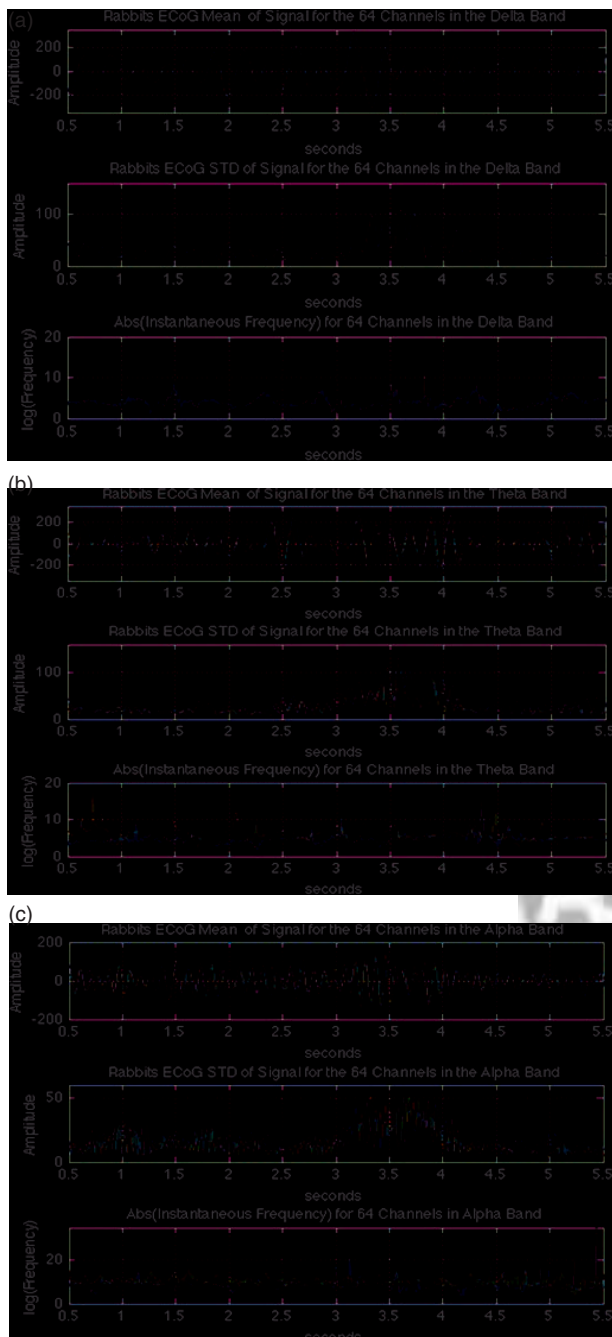
Fig. 9. ECoG signal amplitudes filtered over various temporal frequency bands at constant 2 Hz bandwidth segments; each plot displays the average signal amplitude (SA), standard deviation of the signal (STDx), and the average instantaneous (IFx) frequency over the given narrow band in linear coordinates; (a) delta (2 Hz–4 Hz); (b) theta (4 Hz–6 Hz) and (6 Hz–8 Hz); (c) alpha (8 Hz–10 Hz) and (10 Hz–12 Hz). Multiple curves on a given figure indicate the signals obtained over multiple frequency bands of width 2 Hz each.

Fig. 10. Analytic Amplitude (AA) of the signals after Hilbert transformation; the signals have been filtered over various temporal frequency bands at constant 2 Hz bandwidth segments; each plot displays the average analytic amplitude (AA), standard deviation of the AA, and the average frequency over the given narrow 2 Hz frequency band; (a) delta (2 Hz–4 Hz); (b) theta (4 Hz–6 Hz) and (6 Hz–8 Hz); (c) alpha (8 Hz–10 Hz) and (10 Hz–12 Hz).

3–4 s is significantly different from the rest of the time segments for all frequency bands. In that period, the moments between 3–3.5 s and between 3.5–4 s are also significantly different. Particularly, in the period between 3.25–3.5 s the frequency dispersion drops dramatically around the mean

due to high synchronization. This then is followed by a dramatic increase in dispersion between the period 3.5–4 seconds. These observations clearly point to the onset of significant synchronization during 3.2–3.5 s, which seems to diminish during 3.5–4 s. There may be diminished synchronization during 3.5 Hz to 4 Hz, but it cannot be stated
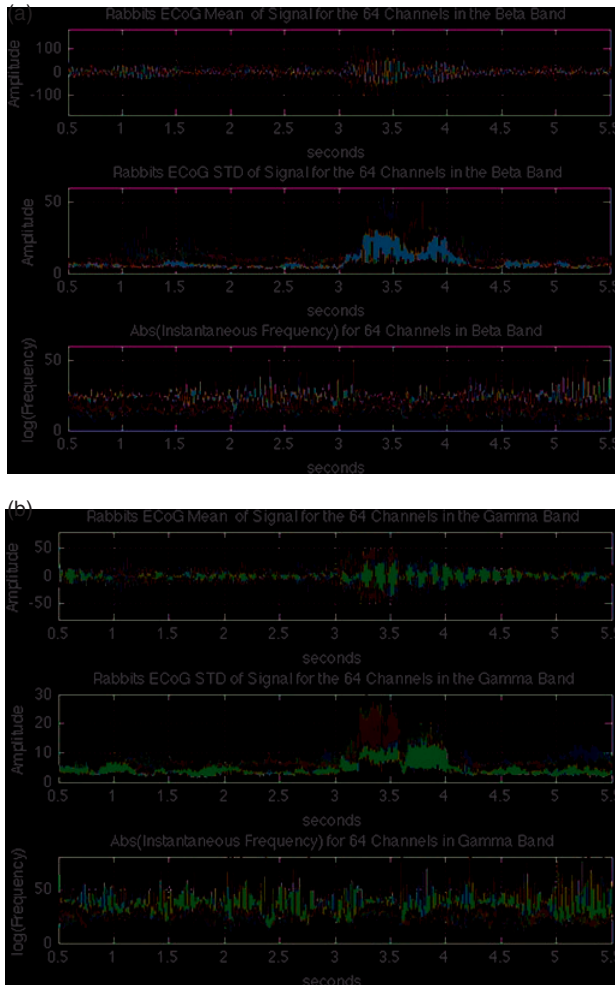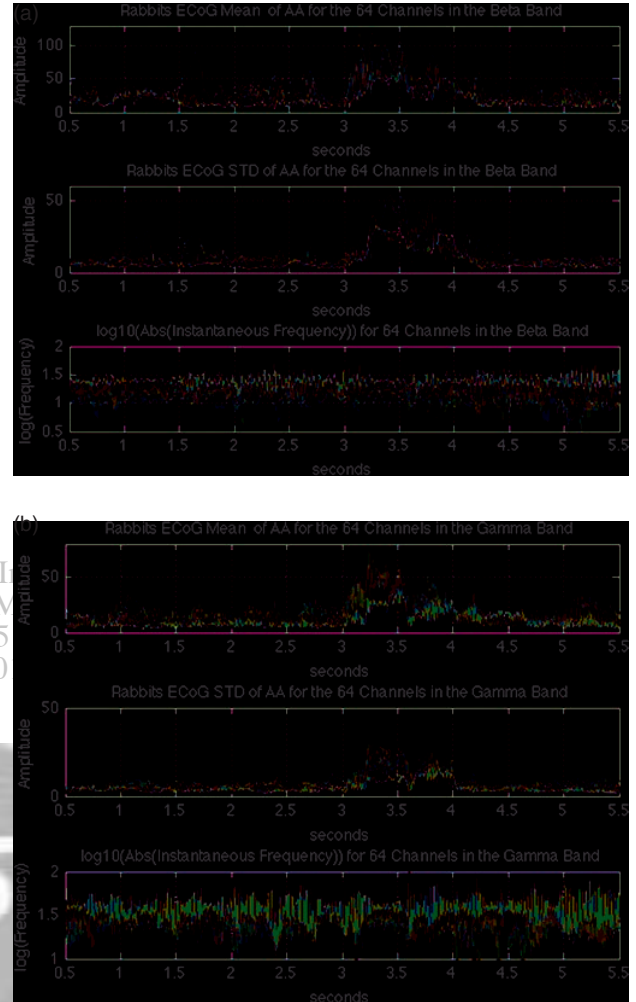
Fig. 11. ECoG signals filtered over various temporal frequency bands at constant 2 Hz bandwidth segments; each plot displays the signal amplitude (SA), standard deviation of the signal, and the average frequency over the given narrow band in linear coordinates; (a) beta (12 Hz–26 Hz) and 2 Hz bandwidth increments; (b) low gamma (26 Hz–40 Hz) at 2 Hz bandwidth. Multiple curves on a given figure indicate the signals obtained over 7 bands of width 2 Hz each.

Fig. 12. Analytic Amplitude (AA) of the signals after Hilbert transformation; the signals have been filtered over various temporal frequency bands at constant 2 Hz bandwidth segments; each plot displays the analytic amplitude (AA), standard deviation of the AA, and the average frequency over the given narrow 2 Hz frequency band in logarithmic coordinates; (a) beta (12 Hz–26 Hz) at 2 Hz increments; (b) low gamma (26 Hz–40 Hz) at 2 Hz increments.

with high confidence due to the indeterminacy of the analytic phase. The AA magnitude remains very high until about 4 s, and suddenly drops afterwards.

The observed effects indicating transitions are the most prominent during the post- stimulus period of 1s in gamma and beta bands; they are also observable though less prominent in the alpha and theta bands. This observation means the presence of an important intra-cortical effect across frequencies 4 Hz to 40 Hz. This effect is not seen in the delta band, below 4 Hz. This may be caused by the absence of significant delta component in the ECoG signal at the given experimental setup. It is important to mention that the average frequency for the 2–4 Hz band is expected around 3 Hz, however, in our analysis we found it to be over 4 Hz. This observation indicates that filtering low frequencies requires careful attention. It is also possible that
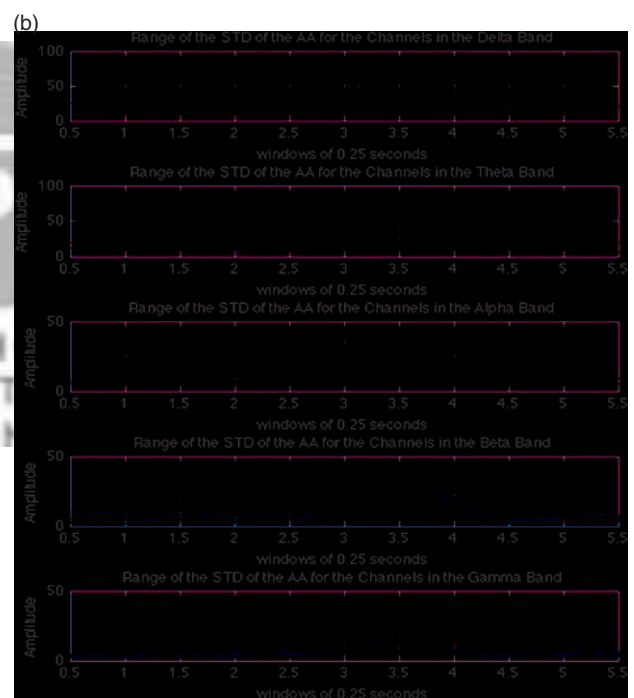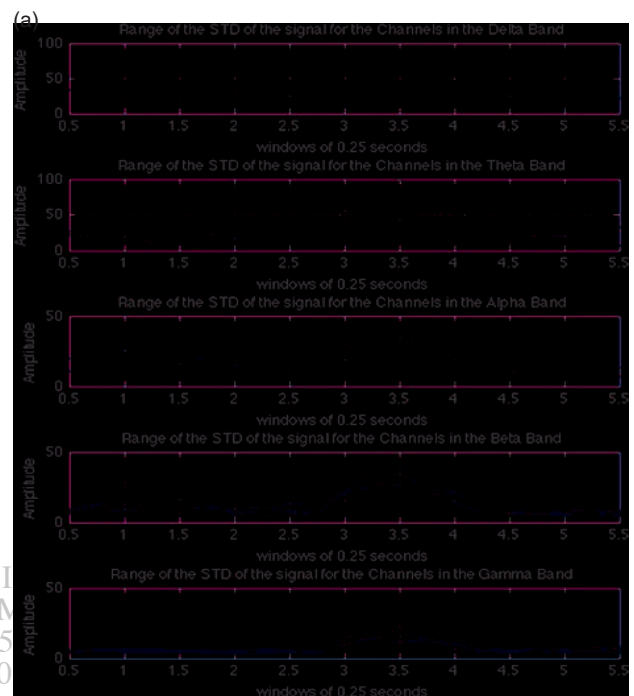
delta frequency band is insignificant or absent during this specific experimental task.

In order to provide further quantitative measures of the observed increase in the oscillations during the post stimulus period, we define the range of oscillations across channels at sliding windows of length 0.25 s. In Figure 13(a) we show the range for the mean of the SA, while Figure 13(b) shows the range of mean for AA. Similarly, Figure 14(a) shows the range for the spatial standard deviation of the SA, while Figure 14(b) shows the same quantity for AA. This analysis allows us to have a measurement of change for windows of time and therefor may help on classifying events and their neural correlates. We observe that the range measure is a suitable index to quantify the increased oscillations during 3–4 s. Again, the delta band indicates less clear response to the classified stimulus.
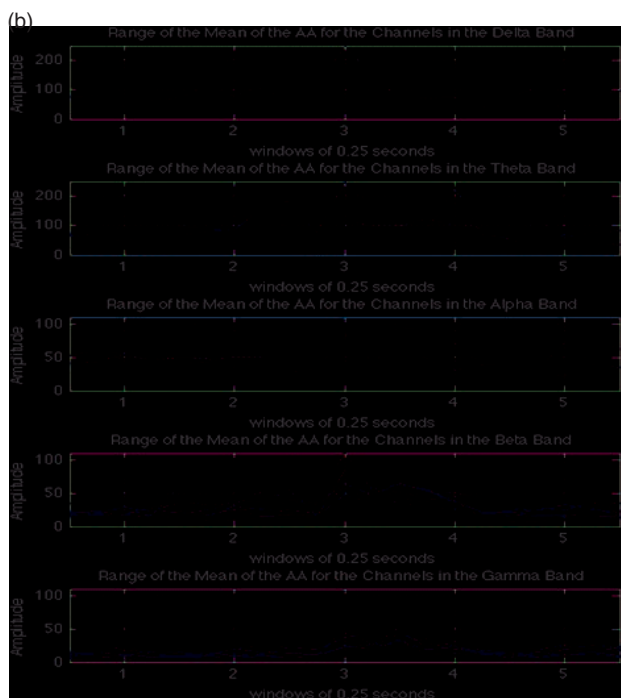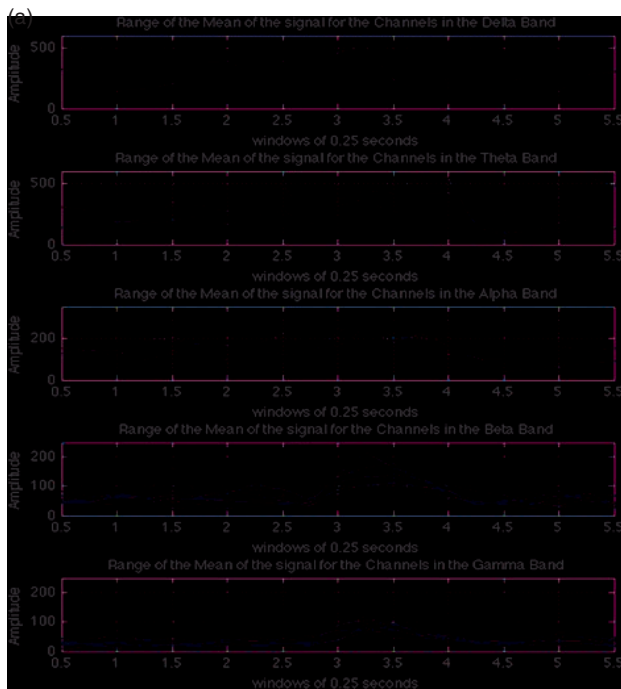
Fig. 13. Range of the mean values over frequency bands delta, theta, alpha, beta, and gamma with window length of 0.25 s; (a) ranges of the ECoG signals; (b) range for the analytic amplitudes (AA).

Fig. 14. Range of the STDx over frequency bands delta, theta, alpha, beta, and gamma with window length of 0.25 s; (a) range for the ECoG signals, (b) range for the analytic amplitudes (AA).

Finally, we return to earlier results obtained for the classification of AM patterns, see Figure 2. Those results indicated that the AM patterns have discriminative power during the first 0.2 s after the stimulus (Type I effect), and towards the end of the 1 s post stimulus period (Type II effect). Looking at the results of our present work, we also see the prominence of the 1 s post stimulus

period, however, the regions of interest seem complementary. Specifically, we see strong synchronization during the 3.25–3.5 s period, which switches to desyncronization during the 3.5–3.75 s period. Note that precisely this is the period when the AM classification did not work! The AM patterns vary rapidly during the intermittency period of 3.25–3.75 s, which may be reason of the absence

of classifiable AM patterns. The present analysis may provide important details exactly during the critical transition period 3.25–3.75 s about the spatio-temporal neurodynamics. This is the decision making period, during which the subject tries to solve the classification task.

A possible interpretation is given as follows: after a brief desynchronization period of approx. 0.2 s, the subject tries to solve the task, which is marked by large-scale cortical synchronization for a period of about 0.3 s. At the end of this 0.3 s period, a possible solution starts to emerge in the form of a new AM pattern. The consolidation of the new AM pattern takes about 0.2–0.3 s. Finally, at 0.8–1 s after the stimulus, a new AM pattern is clearly established and it can be classified successfully. After successful classification, the subject is satisfied and loses interest in the stimulus, thus its brain activity returns to the background level. Obviously, extensive future studies are needed to better understand the observed dynamics and to validate the outlined hypothesis.

CONCLUSIONS AND FUTURE PERSPECTIVES

In this work we analyzed ECoG data and identified synchronization effects with sudden transitions in spatio-temporal neurodynamics. The observed effects can be interpreted based on dynamical systems models. According to dynamical brain theory, destabilization of cortical dynamics can be initiated at some seemingly random point of time and space in the cortex. This phenomenon is similar to phase transition in physical systems, which start at a certain nucleus, like the condensation of vapor to liquid. Phase transitions in brains, however, are much more complex than in physics. In brains, transitions to low-dimensional phase with large-scale synchronization are intermittent and meta-stable, followed by periods of cortical dynamics evolving in a high-dimensional phase. There is a cycle of transitions from low-to-high-to-low dimensions. The collapse of the high-dimensional cognitive space to a low-dimensional subspace of attractors demarcates the intermittent cognitive activity. The global synchronization dynamics indicates the formation of percepts and may serve as an indicator of high-level cognitive experience.

Our analysis points to the cognitive significance of the period between 3–4 s, which is divided into time segments 3–3.5 s and 3.5–4 s. In the first time segment, and in particular during the period 3.25–3.5 s, the frequency dispersion around the mean drops dramatically due to high synchronization across the cortex. This then is followed by a dramatic increase in dispersion between the period 3.5–3.75 s. Both SA and AA range measures seem useful; perhaps AA measures can provide more powerful discrimination. Clearly, future detailed hypothesis tests are required to validate the introduced measures as useful correlates of

classification performance based on the observed ECoG amplitude and phase patterns. We can see that various information-theoretic indexes capture the changes numerically and may be used as neural correlates of cognition and decision making.

We would like to leave the reader with some interesting questions for further research in relation to human awareness, consciousness, spirituality, mental health and ethical behavior, under new emerging paradigms [33]. Could it be that intense eureka or 'aha' moments in scientific research and in philosophical inquiry, or the reported enlightenment moments in religious, spiritual or mystical experience would parallel the observed brief period of desynchronisation followed by a period of intense synchronization and after that a pattern of intermittency, leading to the integration of the experience to a new cognitive map? How could such exploration help people to operate socially closer to a universal framework of ethics, together with the restrictions imposed by habits, addictions, disease and survival needs? Various experimental approaches will be useful to find the answer to these challenging questions [34]. We hope our findings based on EEG analysis motivate further studies towards the identification of neural correlates of cognition and awareness experience through the integration of various experimental paradigms.

References and Notes

1. W. J. Freeman, Consciousness, Intentionality and causality, Reclaiming Cognition: The Primacy of Action, Intention and Emotion, edited by R. Núñez, W. J. Freeman, Bowling Green, OH. Imprint Academic **(1999)**.
2. A. Del Cul, S. Baillet, and S. Dehaene, Brain dynamics underlying the nonlinear threshold for access to consciousness. *PLOS Biology* 5, 2408 **(2007)**.
3. A. K. Seth, Z. Dienes, and A. Cleeremans, Measuring consciousness: Relating behavioral and neurophysiological approaches. *Trends. In Cogn. Sci.* 12, 314 **(2008)**.
4. B. J. He and M. E. Raichle, The fMRI signal, slow cortical potential and consciousness. *Trends in Cogn. Sci.* 13, 302 **(2009)**.
5. C. Koch and G. Tononi, A test for consciousness. *Sci. American* 304, 44 **(2011)**.
6. H. L. Dreyfus, How representational cognitivism failed and is being replaced by body/world coupling, After Cognitivism: A Reassessment of Cognitive Science and Philosophy, edited by K. Leidlmair, Springer, Dordrecht **(2009)**, pp. 39–73.
7. H. L. Dreyfus, Why heideggerian AI failed and how fixing it would require making it more heideggerian. *Artificial Intelligence* 171, 1137 **(2007)**.
8. E. Thompson and F. Varela, Radical embodiment: Neural dynamics and consciousness. *Trends in Cognitive Sciences* 5, 418 **(2001)**.
9. R. Brooks, Flesh and Machine: How Robots Will Change Us, Pantheon, New York **(2002)**.
10. L. W. Barsalou, Grounded cognition. *Annual Rev. Psychol.* 59, 617 **(2008)**.

11. W. J. Freeman, Mass Action in the Nervous System, Academic Press, New York, NY (**1975**).

12. C. Skarda and W. J. Freeman, How brains make chaos to make sense of the world. *Behav. Brain Sci.* 10, 161 (**1987**).

13. P. L. Nunez, Neocortical Dynamics and Human EEG Rhythms, Oxford University Press, Oxford (**1995**).

14. J. A. S. Kelso, Dynamic Patterns: The Self Organization of Brain and Behavior, MIT Press, Cambridge, MA (**1995**).

15. J. J. Wright and D. J. T. Liley, Dynamics of the brain at global and microscopic scales: Neural networks and the EEG. *Behav. Brain Sci.* 19, 285 (**1996**).

16. W. J. Freeman and R. Kozma, Local-global interactions and the role of mesoscopic (intermediate-range) elements in brain dynamics. *Behav. Brain Sci.* 23, 401 (**2000**).

17. G. Werner, Metastability, criticality, and phase transitions in brains and its models. *BioSystems* 90, 496 (**2007**).

18. R. Kozma, T. Huntsberger, H. Aghazarian, W. J. Freeman, Intentional control for planetary rover SRR. *Adv. Robotics* 22, 1309 (**2008**).

19. R. Kozma and W. J. Freeman, Chaotic resonance: Methods and applications for robust classification of noisy and variable patterns. *Int. J. Bifur. Chaos* 11, 1607 (**2001**).

20. W. J. Freeman, Erwin Freeman *K*-set. *Scholarpedia* 3, 3238 (**2008**).

21. J. M. Barrie, W. J. Freeman, and M. Lenhart, Modulation by discriminative training of spatial patterns of gamma EEG amplitude and phase in neocortex of rabbits. *J. Neurophysiol.* 76, 520 (**1996**).

22. W. J. Freeman and J. M. Barrie, Analysis of spatial patterns of phase in neocortical gamma EEGs in rabbit. *J. Neurophysiol* 84, 1266 (**2000**).

23. R. Kozma and W. J. Freeman, Classification of EEG patterns using nonlinear neurodynamics and chaos. *Neurocomputing* 44–46, 1107 (**2002**).

24. R. Kozma and W. J. Freeman, Intermittent spatio-temporal desynchronization and sequenced synchrony in ECoG signals. *Chaos* 18, 037131 (**2008**).

25. R. Kozma, Neural correlates of awareness in brains and man-made devices, *Proc. IEEE Int. Conf. Awareness Science and Technology (iCAST2011)*, IEEE Press (**2011**), pp. 516–520.

26. W. J. Freeman, Origin, structure, and role of background EEG activity. Part 1. Analytic amplitude. *Clin. Neurophysiol*. 115, 2077 (**2004**).

27. Y. Ruiz, S. Pockett, and W. J. Freeman, A method to study global spatial patterns related to sensory perception in scalp EEG. *J. Neurosci. Meth*. 191, 110 (**2010**).

28. J. J. J. Davis and R. Kozma, Analysis of phase relationships in ECoG using hilbert transform and information-theoretic measures, *Proc. IEEE/INNS Int. Joint Conf. Neur. Networks* IJCNN2012/WCCI2012, Brisbane, Australia, June (**2012**).

29. W. J. Freeman, Definition of state variables and state space for brain-machine interface. *Cognitive Neurodynamics* 1, 85 (**2006**).

30. H. Atmanspacher and H. Scheingraber, Pragmatic information and dynamical instabilities in a multimode countinous-wave dye laser. *Can. J. Phys.* 68, 728 (**1990**).

31. W. J. Freeman and R. Q. Quiroga, Imaging Brain Functions with EEG: Advanced Temporal and Spatial Analysis of Electrocorticographic Signals, Springer (**2012**).

32. J. J. J. Davis and R. Kozma, On the invariance of cortical synchronization measures across a broad range of frequencies," *Proc. Int. Conf. Awareness Computing iCAST2012*, IEEE Press, Seoul, Korea, August (**2012**), (In Press).

33. J. J. J. Davis, The Brain of Melchizedek, Thesis, Otago University, Dunedin, New Zealand (**2009**).

34. N. K. Logothetis, What we can do and what we cannot do with fMRI. *Nature* 453, 869 (**2008**).

FEATURED ARTICLE